https://doi.org/10.1007/s12161-021-02099-w

The Advantage of Multispectral Images in Fruit Quality Control for Extra Virgin Olive Oil Production

Diego M. Martínez Gila[1] · Javiera P. Navarro Soto[1] · Silvia Satorres Martínez[1] · Juan Gómez Ortega[1] · Javier Gámez García[1]

Received: 14 December 2020 / Accepted: 23 July 2021

Abstract
The highest quality of extra virgin olive oil must be guaranteed to succeed in the competitive market of the industry. To fulfil this need, high standards of fruit quality are required. In recent years, this search has led to the development of computer vision systems for the automatic inspection of fruits. Skin damage, dirtiness, and external colour were the main features selected. However, no known report is related to the internal quality evaluation of olives. The present research explores the application of multispectral images (from 600 to 975 nm) to discriminate olive fruits by their firmness. To achieve this aim, 58 olives were classified as hard or soft by an expert and then measured by a penetrometer. Afterwards, 58 multispectral images were obtained, and 8352 pixels were randomly selected for feature extraction. The feature vector of each pixel was composed of 25 infrared absorption values. These data were input into three supervised classification algorithms: a naïve Bayes (NB) classifier, a multilayer perceptron (MLP), and a support vector machine variation (SMO). The highest performance was achieved by the MLP, with an accuracy of 95% for the firmness grading. Furthermore, the three algorithms were subjected to principal component analysis (PCA), by which the MLP was confirmed to be the best model and its results were improved. Moreover, according to the second principal component, the 675 nm and 855 nm band frequencies have the strongest weights. The overall results confirm the convenience of multispectral imaging in olive firmness inspection, with the advantage of being a non-invasive technology.

Keywords Multispectral image · Olive fruits · Automatic · Pattern recognition · Firmness

Introduction

In the competitive market of the extra virgin olive oil (EVOO) industry, it is necessary to guarantee the highest quality of the products. For this purpose, the olive fruits must fulfil high standards of quality, as they play a major role in the production process.

Currently, to ensure that the raw materials have the required quality, the EVOO industry is beginning to introduce different sensors along the processing line for the quality control of the incoming fruit. In this regard, computer vision has the benefits of being a non-invasive technology, with the advantage of providing online and timely information during continuous work (Zhang et al. 2014). Studies in this field have made progress in terms of different inspection models in the last few years. In general, computer vision applications for the EVOO industry are distributed between those able to discriminate olive batches by external colour (Furferi et al. 2010; Ram et al. 2010; Avila et al. 2015) and those able to discriminate olive batches by skin or pest damage (Riquelme et al. 2008; Guzmán et al. 2013). There are also models that are able to differentiate olive batches according to their dirtiness, which include foreign element contamination such as sticks or stones (Aguilera et al. 2015).

In a recent study, researchers (Navarro et al., 2018) successfully correlated quality parameters and oil nutritional values through RGB images from olive batches. In that work, in addition to the colour feature, the texture feature was selected with the idea of showing internal firmness differences, resulting in a decline in the oils produced with soft fruits. To avoid the risk of declining oil quality, the

✉ Diego M. Martínez Gila
dmgila@ujaen.es

[1] Robotics, Automation and Computer Vision Group, University of Jaén, Campus Las Lagunillas s/n, 23071 Jaén, Spain

International Olive Council (2011) suggests collecting fruit at early ripening stages, defined as a skin colour between green and purple with white flesh. At these stages, hard fruits are able to better resist transport and storage (Zhang et al. 2014) by being less prone to skin damage than soft fruits (Kalua et al. 2007). The downside of collecting these fruits early is that extra force is required to detach them from the tree, increasing the harvesting difficulty and cost (Beltrán et al. 2008). Additionally, at these early ripening stages, fruits are composed of less internal water, hindering oil extraction (Di Giovacchino 2000). Consequently, a decline in profitability is expected in the production of EVOO from early ripe olives (Cano Marchal et al. 2014). Conversely, later in the ripening process, fruit detachment from trees occurs easily, and ripe fruits facilitate oil extraction. Notwithstanding, the main inconvenience of the ripe olives to be considered in the extraction of EVOO is the lack of firmness that the fruits might have. Usually, olives in advance maturity stages are susceptible to damage during transportation or gathering. Any damage to the olive skin exposes the pulp, risking oil quality reduction due to fermentation, which should be avoided during EVOO production (Angerosa et al. 2004).

Nevertheless, there is a stage in which ripe olives, which are completely black on the outside, sustain an optimum internal firmness; this condition represents an opportunity to obtain a high-quality EVOO within high yields. However, these fruits are left over during low-quality oil production due to the impossibility of discriminating between olives that seem the same from the outside, that is, totally black, but have a completely different internal pulp firmness.

Beyond the fact that soft fruits are prone to damage along the production chain, there are some inner changes related to the loss of firmness that might potentially affect the oil quality. The firmness decline involves cell wall separation, including the degradation or solubilization of main constituents, resulting in purple-black pulp in addition to all other modifications (Mafra et al. 2001; Kafkaletou et al. 2019). Eventually, cell wall separation creates a path for encountering sugar compounds, oil drops, and free water, creating the worst-case scenario, in which the fermentation process begins and ruins the oil quality (Vicente et al. 2007).

A relatively recent technology, hyperspectral imaging, has proven to be suitable for fruit inspection under the surface, with possibilities to be useful in identifying firmness differences. The first studies using hyperspectral images, which began over a decade ago, successfully identify areas in cucumbers affected by bruises (Ariana et al. 2006). Years later, experiments confirmed with accurate results the firmness evaluation with hyperspectral images of blueberries, which are characterized by being totally black during the ripening process (Leiva-Valenzuela et al. 2013). Nonetheless, the penetrometer continues to be the standard instrument for firmness evaluation, with the inconvenience of being a destructive method, measuring the resistance of a force applied over the fruit surface (Xu et al. 2019). This invasive methodology evaluates only a few samples. Therefore, hyperspectral imaging represents an opportunity for quality control in a large range of fruits and vegetables, for firmness evaluation and even to show bruises that might indicate mishandling during transportation. This kind of sensor has the possibility of detecting modifications in the cell and intracellular wall structures by analysing the light absorption at different near-infrared wavelengths (Sun et al. 2016). Even so, the effectiveness of this technology in firmness determination will depend on the skin surface thickness and on the pulp properties of the element to be inspected (ElMasry and Sun 2010). Until now, hyperspectral technology has led a series of studies with excellent performance on firmness classification models applied to plum, nectarine, pear, strawberry, and kiwi fruits (Zhang et al. 2016; Zhu et al. 2017; Li et al. 2018; Yu et al. 2018; Munera et al. 2019).

One of the advantages of hyperspectral images is the immense number of wavelengths that can be captured. This technology integrates not only the spectroscopy principles but also the spatial region information of each pixel (ElMasry and Sun 2010). This property also means subsequent large spectral data, increasing the cost of the sensor and consequently the runtime of the analysis (Hussain, Pu and Sun, 2018). With the intention of outstripping these disadvantages, research has focused on multispectral cameras. By having the same technology, although with fewer spectrum wavelengths, multispectral sensors achieve a quicker data analysis and therefore are more suitable for industry implementation (Zhang et al. 2014). Comparing the two technologies, in the case of apple firmness determination, hyperspectral images achieve a better performance by selecting a group of wavelengths than with the total bands available (Zhu et al. 2013). Moreover, a perfect firmness determination was achieved by a multispectral device, also in apple fruits (Sun et al. 2016).

To the best of our knowledge, no studies have been performed with the object of computer vision to identify the internal changes in the pulp of olive fruits. In this research, we propose a multispectral imager as a suitable sensor to capture the inside firmness differences in ripe olives. To achieve this aim, an expert will sort black olives into two groups, soft and hard fruits, and then firmness of each fruit will be measured by a penetrometer. Afterwards, images will be captured individually, and the resulting data will be evaluated with three different algorithms, namely, naïve Bayes (NB), multilayer perceptron (MLP), and support vector machine, based on sequential minimal optimization (SMO), for training. Furthermore, to improve the general performance, principal component analysis (PCA) will be

applied to the data source prior to the application of the classification methods.

Materials and Methods

Experimental Samples and Treatment

The olive fruits were obtained from the same tree belonging to the University of Jaén (GPS coordinates: 37° 47′ 24.44″ N, 3° 46′ 45.5″ W) whose variety is *Picual*. The selected tree is used only for research purposes, receives no chemical treatments, and was reserved for the experiment.

Fruit samples were collected on the same day, 21 February 2019, at the end of the harvest period when there were few fruits left on the tree due to rain and wind. Of all the olives available on the tree, the candidates to be harvested were those that did not present external imperfections such as insect bites or the presence of fungi. At the time of sampling, most of the olives that remained on the tree were soft olives. Therefore, the number of samples in the experiment was limited by the number of hard olives that remained on the tree. Thus, the total number of samples was 58.

The fruits were collected by hand picking, avoiding any damage related to mechanical harvest or transport. The whole set of olive samples was completely black without external differences. First, the fruits were divided in two groups:

- The first group was composed of olives that were hard to the touch at the time of harvest. Thirty-four olive fruits were assigned to the hard class.
- The second group was composed of olives that were soft to the touch at the time of harvest. Twenty-four olive fruits were assigned to the soft class.

The criterion followed for this first classification was that of the person who was in charge of collecting the olive samples. Since this procedure could not be objective, it was decided to confirm the classification made through a measuring instrument. Then, both groups of olives were submitted to firmness determination by a standard firmness instrument, a penetrometer (model GY-2 from YJINGRUI®) using a head diameter of 11 mm. This instrument also has a resolution of 0.2 mm and a measurement range of $4*10^5$ Pa. An example of an evaluation of an olive with the penetrometer is shown in Fig. 1. The procedure was to measure the olives one by one. To do this, the tip of the penetrometer is placed on the skin of the olive. At that moment, we begin to press the instrument against the olive until the skin breaks and the tip penetrates into the olive. The value that marks the instrument just before penetrating is the data that is collected.

Fig. 1 The measurement process with the penetrometer device

The measurement results performed by the penetrometer for each olive are shown in Fig. 2. The resistances differences are clearly apparent between the two studied groups. Hard fruits present a higher resistance than soft fruits to penetrometer action.

An accurate definition of these groups is shown in Table 1, where the mean, standard deviation and mode are presented. In the same table, the maximum and minimum values for each group denote a clear difference in the firmness between them.

The drop in firmness might indicate the beginning of extensive enzymatic activity and free radicals that degrade the cell texture or solubilize the cell walls (Guillén, Fernández-Bolaños and Heredia, 1993; Ana Jiménez et al. 2001; Kafkaletou et al. 2019).

Image acquisition

Images were acquired individually for each olive fruit using an ad hoc hardware setup. A white background was installed under the tray. Images were acquired by means of a multispectral Photonfocus A1312 camera based on a CMOSIS 2 Megapixel CMOS sensor with 5×5 mosaic filters and a full-width half-maximum (FWHM) of 15 nm. The main feature of this device is that each pixel is composed of 25 subpixels, where each subpixel acquires light information of a wavelength in the infrared spectrum using 25 band-pass filters from 600 to 975 nm. The spatial resolution of the sensor is 409×217 pixels per spectral band. The camera with a 35-mm lens was positioned 640 mm from the sample. The lighting system consisted of a 125 W halogen lamp placed in the camera optical axis. The halogen lamp was selected based on previous experimental tests in which the stability and gain in the response of the multispectral camera sensor were observed. Figure 3 shows the image acquisition setup. Once the setup was configured,

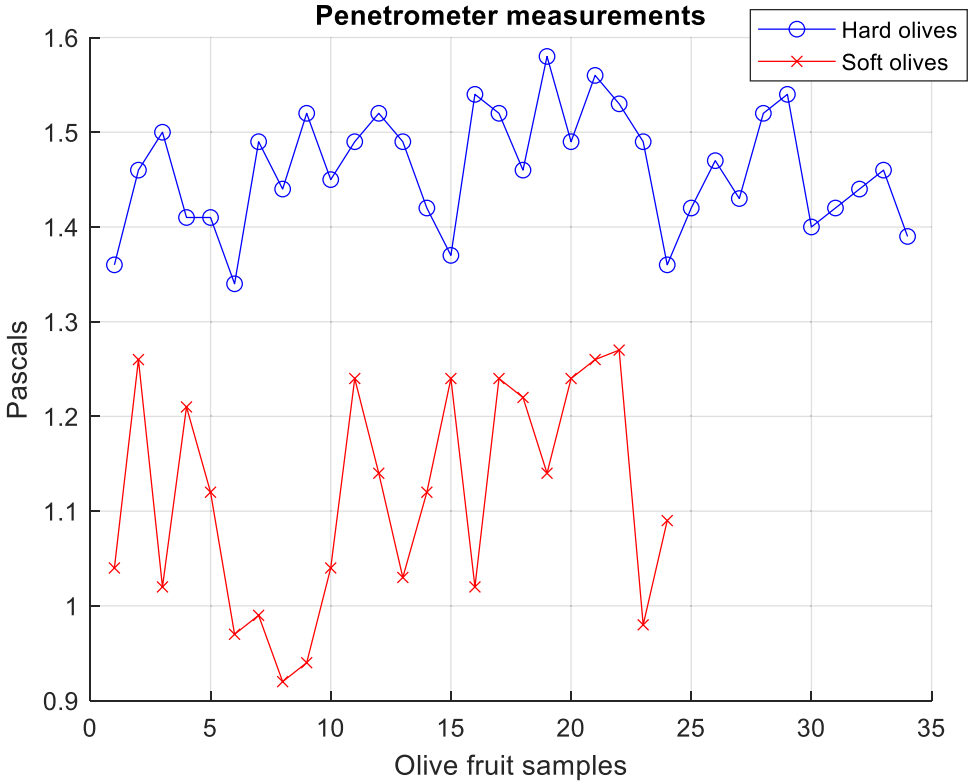

Fig. 2 Graphic representation of the penetrometer results over the studied olive *groups*

Table 1 Results after measurements with the penetrometer

Olives	Mean	Stand. dev	Stand. error	Mode	Max	Min
Hard	1.46	0.06	0.010	1.49	1.58	1.34
Soft	1.10	0.11	0.018	1.24	1.27	0.9

58 multispectral images were captured, one for each olive. For each olive fruit, the procedure was as follows:

1. An olive is extracted from the set.
2. The olive is placed in the field of view of the multispectral camera that is capturing in continuous mode.
3. Through the vision software, it is checked that the olive is correctly located.
4. Finally, the image is frozen and saved as an image file in BMP format.
5. The inspected olive is removed from the camera's field of vision and if there are olives left in the set, go back to step 1.

Image Processing and Features Extraction

Once acquired, each multispectral image was corrected according to Eq. 1.

$$I_s^{cor}(n,m) = \frac{I_s^{orig}(n,m) - B(n,m)}{W(n,m) - B(n,m)} \quad (1)$$

where $I_s^{cor}(n,m)$ is the corrected multispectral image, $I_s^{orig}(n,m)$ is the original multispectral image, $B(n,m)$ is the black image obtained by closing the iris of the camera (approximately 0% reflectance), and $W(n,m)$ is the white image obtained from a white Teflon sheet (approximately 99% reflectance). In addition, n and m represent the number of pixels in the image (n ranges from 0 to 1084, and m ranges from 0 to 2046), and s is the number of samples.

The next step was to extract the 25 infrared channels from each $I_s^{cor}(n,m)$ multispectral image according to Eq. 2.

$$I_s(p,q,c) = \begin{cases} I_s^{cor}(5*p, 5*q+c), 0 \le c < 5 \\ I_s^{cor}(5*p+1, 5*q+c-5), 5 \le c < 10 \\ I_s^{cor}(5*p+2, 5*q+c-10), 10 \le c < 15 \\ I_s^{cor}(5*p+3, 5*q+c-15), 15 \le c < 20 \\ I_s^{cor}(5*p+4, 5*q+c-20), 20 \le c < 25 \end{cases} \quad (2)$$

where $I_s(p,q,c)$ is a three-dimensional image; p and q denote the spatial dimension; and c is the number of infrared channels (ranging from 0 to 24).

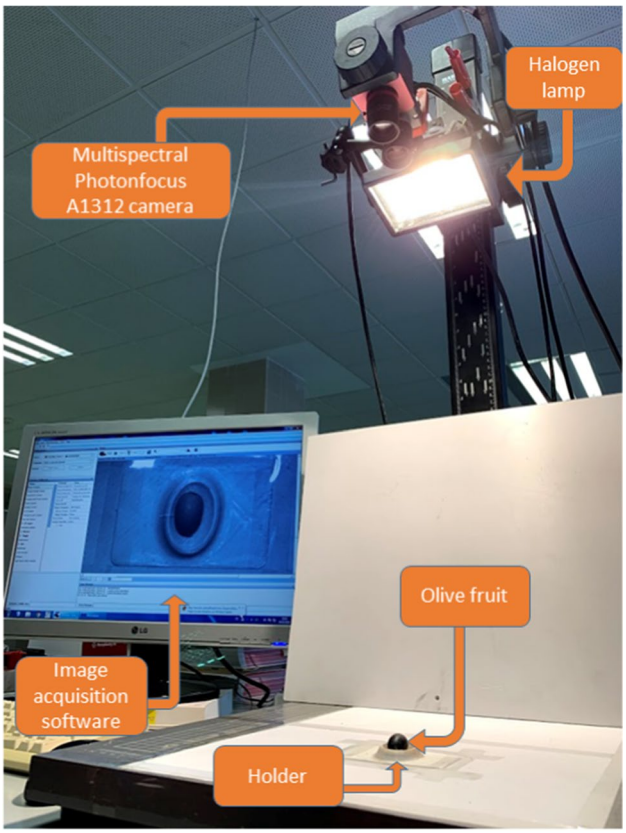

Fig. 3 Image acquisition setup

Afterwards, the goal was to separate the fruit region of the image from the background. For this step, the first task was to compress the information of the different infrared channels into a two-dimensional image averaging the 25 channels for each pixel, which was performed according to the Eq. 3.

$$\bar{I}_s(p,q) = \frac{\sum_{c=0}^{24} I_s(p,q,c)}{25} \tag{3}$$

Second, to extract olives from the $\bar{I}_s$ images, a global threshold binarization algorithm was used, and the threshold was heuristically fixed. The resultant image was the logical mask (M_s) for the olive region, and it was applied to the original images through the logical AND operator (Eq. 4). Additionally, the inverse of the logical mask ($\overline{M_s}$) was applied to the same $\bar{I}_s$ images to extract the background (Eq. 5). The result for each step can be seen in Fig. 4.

$$\bar{I}_s^{fruit}(p,q) = \bar{I}_s(p,q) x M_s(p,q) \tag{4}$$

$$\bar{I}_s^{bg}(p,q) = \bar{I}_s(p,q) x \overline{M_s}(p,q) \tag{5}$$

.

Finally, the matrix $X_s(p \cdot q, m)$ was created for each olive image. This matrix contains the reflectance values for each infrared channel (from 0 to 24) as the columns and for each pixel number (from 0 to $p \cdot q$) as the rows. This matrix was particularized for the olives (Eq. 6) and for the background (Eq. 7).

$$X_s^{fruit}(p \cdot q, m) = \left[I_s(p,q,0), I_s(p,q,1), \ldots, I_s(p,q,24)\right] \quad \text{if } \bar{I}_s^{fruit}(p,q) \neq 0 \tag{6}$$

$$X_s^{bg}(p \cdot q, m) = \left[I_s(p,q,0), I_s(p,q,1), \ldots, I_s(p,q,24)\right] \quad \text{if } \bar{I}_s^{bg}(p,q) \neq 0 \tag{7}$$

After that, principal component analysis (PCA) (Wold et al., 1987) was applied to X_s^{fruit} and X_s^{bg} to reduce the number of features by selecting a linear combination of those feature that explain the variance in the whole dataset. These components were ranked according to the explained variance, and the number of selected components was increased from 1 to 10. In each iteration, the different classification algorithms were evaluated.

Fig. 4 Image processing step

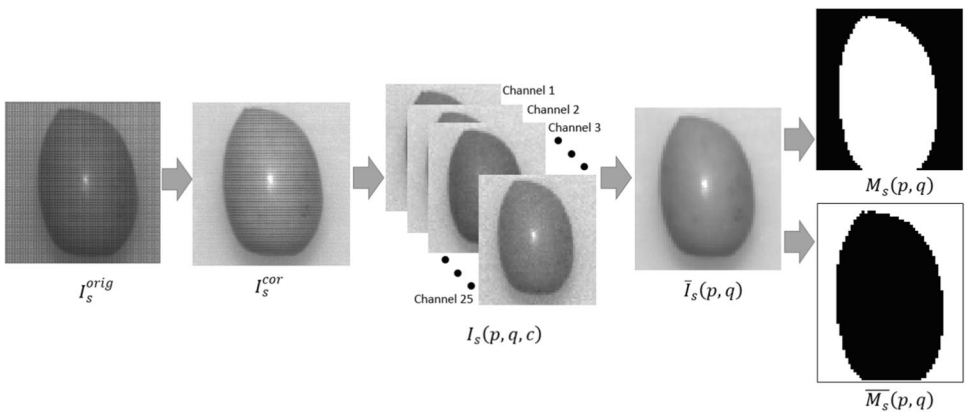

Classification Algorithms

To evaluate the feasibility of using a multispectral infrared camera as a non-invasive post-harvest sensor to classify olive fruits according to their firmness (hard or soft), three supervised classification algorithms were tested: the NB, MLP, and SMO classifiers.

The NB classifier (John and Langley 2013) is a probabilistic classification method and is based on obtaining the probability of belonging to each class of olives in our context. Since the extracted features of olive images (reflectance in the infrared channels) are normally distributed continuous variables, the distribution of each class can be represented as a Gaussian probability density function in terms of its mean μ_c and standard deviation σ_c. In this way, the probability of belonging of each sample to each class will be given by Eqs. 8 and 9.

$$p\left(x_s(p\cdot q,m)|c\right) = g\left(x_s(p\cdot q,m);\mu_c,\sigma_c\right), where \tag{8}$$

$$g\left(x_s(p\cdot q,m);\mu_c,\sigma_c\right) = \frac{1}{\sigma_c\sqrt{2\pi}}e^{-\frac{(v-\mu_c)^2}{2\sigma_c^2}} \tag{9}$$

where $g\left(v_{n,s\times f};\mu_c,\sigma_c\right)$ is the Gaussian probability density function for class c.

Additionally, the MLP classifier was evaluated (Duda, Hart, & Stork, 2001). The MLP classifier is a neural network formed by multiple layers and has the advantage of being able to solve classification problems where the classes are not linearly separable. In our case, the MLP network was configured with three layers: an input layer with 25 nodes (equal to the number of infrared channels), a hidden layer with 58 nodes with sigmoidal transfer functions, and an output layer with 3 nodes (equal to the number of classes). The network was trained via backpropagation, and the number of iterations used to train the MLP was 500.

The last classifier was SMO, which is an algorithm for training support vector machines (Cortes and Vapnik, 1995). The main idea is to find the hyperspace where our considered classes could be optimally separated. This approach is based on a decision boundary that can be described as a hyperplane that is expressed in terms of a linear combination of functions parameterized by support vectors that give the best separating hyperplane using a kernel function (Eqs. 10 and 11).

$$\min_{\beta,\beta_0}\frac{1}{2}\|\beta\|^2 + C\sum_{i=1}^{N}\xi_i \tag{10}$$

$$\text{subject to } y_i\left(x_i^T\beta+\beta_0\right) \geq 1-\xi_i \forall i \tag{11}$$

The method used to validate the classification algorithms was the well-known hold-out method. It consists of dividing the data set into a "train" and "test" set. The training set is what the model is trained on, and the test set is used to see how well that model performs on unseen data. In our case, the percentages applied were 50–50; that is, half of the images were used for training and the other half for validation. The results will be evaluated based on a confusion matrix, as shown in Fig. 5.

The performance of the classification models was assessed in terms of true positive (TP) rate, false positive (FP) rate, precision, recall, F-measure, Matthews correlation coefficient (MCC), receiver operating characteristic (ROC) curve, and precision-recall curve (PRC). The TP rate is the percentage of observations that have been assigned to an evaluated class when they truly belong to that class; the higher this value is, the better the result. The FP rate is the percentage of observations that have been assigned to a certain class when they do not truly belong to that class; the lower this value is, the better the result. The precision is the ratio of correctly predicted positive observations to the total number of predicted positive observations (Eq. 12); the recall is the ratio of correctly predicted positive observations to all the observations in the evaluated class (Eq. 13). The F-Measure is the weighted average of the precision and recall (Eq. 14). The MCC is a measure of the classification quality. It returns a value between −1 and 1, where 1 represents a perfect prediction (Eq. 15). The ROC curve represents the relation between the true positive rate and false positive rate; the PRC shows the relationship between the precision and recall. The higher the ROC and PRC curves are, the better the classification model.

$$Precision = \frac{TP}{TP+FP} \tag{12}$$

		Predicted class by the model	
		Evaluated class	Other classes
Real class	Evaluated class	TP	FN
	Other classes	FP	TN

Fig. 5 Confusion matrix obtained for each evaluated class. TP is the number of true positives, FN is the number of false negatives, FP is the number of false positives, and TN is the number of true negatives

$$Recall = \frac{TP}{TP + FN} \tag{13}$$

$$F - Measure = \frac{2 \times (Recall \times Precision)}{Recall + Precision} \tag{14}$$

$$MCC = \frac{TP \times TN - FP \times FN}{\sqrt{(TP + FP) \times (TP + FN) \times (TN + FP) \times (TN + FN)}} \tag{15}$$

Results and Discussion

The classifiers will be evaluated by their performance to distinguish among pixels belonging to multispectral images of soft fruits (class 1), those that belong to hard olives (class 2), and those that belong to background (class 3). The pixels to train and subsequently validate the classification models were randomly extracted from the olive fruit surface for classes 1 and 2 and from the background of the images for class 3. The total number of olive fruit images was 58 (34 hard olives and 24 soft olives). Of these, 29 olives were used to train the models, and the remaining 29 olives were used for validation. Finally, the total number of pixels selected from these images was 8352. Six matrices were created from the selected pixels, three of them for training (one per class) and the other three for validation (one per class):

- $X^{c1\_t}_{1152,25}$, $X^{c2\_t}_{1632,25}$, and $X^{c3\_t}_{1392,25}$: These matrices contain the infrared absorption values of the pixels used to train the classification models. Specifically, 1152 pixels were used to train class 1, 1632 pixels were used to train class 2, and 1392 pixels were used to train class 3.
- $X^{c1\_v}_{1152,25}$, $X^{c2\_v}_{1632,25}$, and $X^{c3\_v}_{1392,25}$: These matrices contain the infrared absorption values of the pixels used to validate the previously trained classification models. The number of pixels used to validate the models was the same as that used to train them.

After training the models and validating them, the classification results obtained were those that appear in Table 2. The results identified the MLP algorithm as the most suitable algorithm, with an average TP rate above 0.95. This finding means that 3984 pixels were correctly classified and only 192 pixels were misclassified. The best precision value was obtained for class 3 (background). In this case, all the pixels were perfectly classified with a true positive rate or 100%. This result could be useful in image segmentation processes where olive fruits need to be separated from the background. For example, the objective of Ponce et al. (2019) was to count the number of olives that are present in a batch of olives. For this purpose, the authors needed to have additional lighting (backlighting) to be able to separate the background from the image of the olives.

The next step was to perform principal component analysis (PCA) to increase the TP rate for classes 1 and 2. Then, PCA was applied to the training dataset. The graphical results in the PCA space can be seen in Fig. 6. The percentage of the total variance explained by the first two principal components was 98.83%. The scores of the PCA are shown in Fig. 6a, where the differences between classes are clearly visible. Moreover, Fig. 6b presents the PCA loadings, which show the contribution of each infrared channel. According to the second PCA, infrared channels 5 (675 nm) and 17 (855 nm) have more weight than the others. In other words, the experimental setup could be made cheaper by replacing the multispectral camera with an infrared camera with an optical filter located at one of the two wavelengths and the results would be similar. The same band at 675 nm was probed to be important to denote bruises in strawberries (Liu et al. 2018). Moreover, other experiments have concluded that the closest band at 680 nm relates to firmness declination for pears and apples.

Table 2 Classification parameters results for the three different algorithms

Algorithm	Class	TP rate	FP rate	Precision	Recall	F-measure	MCC	ROC	PRC
NB	1	0.864	0.09	0.785	0.864	0.822	0.752	0.95	0.902
	2	0.804	0.06	0.896	0.804	0.847	0.76	0.951	0.899
	3	0.995	0.021	0.96	0.995	0.977	0.966	0.992	0.971
	Average	0.884	0.055	0.886	0.884	0.884	0.826	0.965	0.924
MLP	1	0.931	0.037	0.905	0.931	0.918	0.887	0.982	0.962
	2	0.931	0.031	0.951	0.931	0.941	0.904	0.987	0.978
	3	1	0	1	1	1	1	1	1
	Average	0.954	0.022	0.955	0.954	0.954	0.931	0.99	0.981
SMO	1	0.865	0.022	0.938	0.865	0.9	0.865	0.953	0.867
	2	0.958	0.061	0.909	0.958	0.933	0.889	0.949	0.888
	3	1	0.001	0.999	1	0.999	0.999	1	0.999
	Average	0.946	0.03	0.947	0.946	0.946	0.919	0.967	0.919

Fig. 6 PCA-2 results

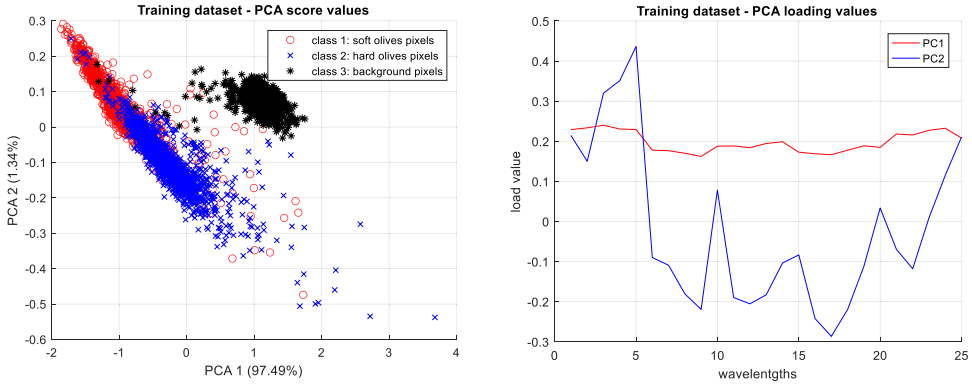

Finally, the validation dataset was also transformed to the new PCA space with the previously obtained loadings. This operation was applied using from 1 to 10 principal components. Consequently, 10 training models were evaluated and validated for each classification method. In total, 30 models were tested, and we referred to them according to the PCAX-METHOD format, where X is the number of main components considered (from 1 to 10) and METHOD is the classification method considered (NB, MLP, or SMO).

The maximum values of the accuracy for the first ten components varied among the three algorithms evaluated. In general, the PCA7-NB model had the lowest performance, obtaining 95.1%. An improvement in the performance was found in the PCA7-SMO model with an accuracy of 95.31%. The highest accuracy was obtained with the PCA9-MLP model, with a maximum of 96.31%. Finally, the confusion matrix for the PCA9-MLP model is presented in Table 3. In this table, it can be seen that 93 pixels were erroneously classified as hard class and 61 pixels were erroneously classified as soft class. This is because all the pixels in the olive do not have the same degree of firmness. In other words, an olive classified as soft can have 90% of its surface soft and the remaining 10% hard.

These results confirm the convenience of the multispectral camera for quality control to discriminate ripe olives by their firmness with great precision. At industrial level, continuous inspection systems based on computer vision are being investigated as a utility for the characterization of the fruit at the entrance of the process. For example, in the work documented in Aguilera Puerto et al. (2019), the authors propose a setup that, installed in the oil mills, allows the continuous characterization of olive batches. The classification is made based on the amount of dirt that the batch presents. The multispectral technology that has been documented in this work could complete the continuous system. With this technology implemented online, soft fruits could be left aside, avoiding oil quality diminishment due to susceptibility to injury during shipment or storage and pathogen attacks (Vicente et al. 2007). Conversely, being able to recognize olive fruits that maintain their firmness would increase the profitability of the industry. Ripe olives in perfect health condition have the potential to produce high-quality EVOO with more sweet and aromatic flavours such as nut and ripe fruit flavours (Kalua et al. 2007). The task of determining the firmness of olives could not be carried out at an industrial level using a penetrometer due to the slowness of the procedure and the large quantity of olives that are received in the oil mills.

In emergent markets, these oils might have better acceptance than those produced with early green fruits, which have a higher bitterness and pungency and are not usually easily accepted by new consumers (Fernandes et al. 2018).

Table 3 Results of the PCA9-MLP model

PCA9-MLP		Predicted class		
		Soft	Hard	Background
Real class	Soft	1059	93	0
	Hard	61	1571	0
	Background	0	0	1392

Conclusions

This work has documented the application of a multispectral camera for internal quality control in ripe black olives. The work of this automatic computer vision sensor reaches wavelengths between 600 and 975 nm. The three different algorithms (NB, MLP, and SMO), which were employed for firmness evaluation, generally showed a good response. However, the MLP algorithm achieved the best execution with a TP rate of over 95% by using hold-out validation. Moreover, in the three algorithms subjected to PCA, an improvement in the results is reflected, although the MLP classifier remains the best classifier. In view of the results,

it has been possible to demonstrate that the three classes to be evaluated, that is, soft olives, hard olives, and the background, are separable with an accuracy of 96.31% in the best case. In terms of wavelength, two wavelengths (675 nm and 855 nm) were those suggested to have the strongest weights in the olive pulp firmness determination. This research exposes the positive application of multispectral technology for the assessment of internal conditions in olive fruits, which have not been considered until now. The integration of the proposed sensor, as an automatic inspection system based on images, in a reception line of olives could be helpful to ensure EVOO quality and to enlarge the quantity of EVOO extracted from firm, ripe olives.

Funding This work has been partially supported by the project of the Ministry of Spain with reference PID2019-110291RB-I00. The authors thank the oil mill Picualia (www.piculia.com) for the olive samples provided to carry out this study. Also we are very thankful for the financial support provided by the Spanish Ministry of Economy and Competitiveness (Precommercial public procurement Innolivar) Exp. 2018/00001, co-funded by European FEDER funds, and the financial support provided by the Interprofessional Organization of Table Olive and Olive Oil, Spain https://interaceituna.com/.

Declarations

Ethical approval This article does not contain any studies with human participants or animals performed by any of the authors.

Informed consent Informed consent not applicable.

Conflict of interest Author Diego M. Martínez Gila declares that he/she has no conflict of interest. Author Javiera P. Navarro Soto declares that he/she has no conflict of interest. Author Silvia Satorres Martínez declares that he/she has no conflict of interest. Author Juan Gómez Ortega declares that he/she has no conflict of interest. Author Javier Gámez García declares that he/she has no conflict of interest.

References

Aguilera D et al (2015) Sorting olive batches for the milling process using image processing. Sensors 15(7):15738–15754. https://doi.org/10.3390/s150715738

Aguilera Puerto D et al (2019) Online system for the identification and classification of olive fruits for the olive oil production process. J Food Meas Charact 13(1):716–727. https://doi.org/10.1007/s11694-018-9984-0

Jiménez A et al (2001) Olive fruit cell wall: degradation of cellulosic and hemicellulosic polysaccharides during ripening. J Agric Food Chem 49(4):2008–2013. https://doi.org/10.1021/JF000809V

Angerosa F et al (2004) Volatile compounds in virgin olive oil: occurrence and their relationship with the quality. J Chromatogr A 1054(1–2):17–31. https://doi.org/10.1016/j.chroma.2004.07.093

Ariana DP, Lu R, Guyer DE (2006) Near-infrared hyperspectral reflectance imaging for detection of bruises on pickling cucumbers. Comput Electron Agric 53(1):60–70. https://doi.org/10.1016/J.COMPAG.2006.04.001

Avila F et al (2015) A method to construct fruit maturity color scales based on support machines for regression: Application to olives and grape seeds. J Food Eng 162:9–17. https://doi.org/10.1016/j.jfoodeng.2015.03.035

Beltrán G et al (2008) Maduración. In: Barranco D, Fernandez-Escobar R, Rallo L (eds) *El Cultivo del Olivo*. Mundi-Pren. Junta de Andalucia, Madrid, pp 165–187

Cano Marchal P et al (2014) Optimal Production Planning for the Virgin Olive Oil Elaboration Process. IFAC Proceedings Volumes 47(3):8921–8926. https://doi.org/10.3182/20140824-6-ZA-1003.02203

Di Giovacchino L (2000) Technological aspects. In: Harwood JL, Aparicio R (eds) Handbook of olive oil: analysis and properties. ASPEN, Gaithersburg, pp 17–59. https://doi.org/10.1007/978-1-4757-5371-4

ElMasry G, Sun DW (2010) 'Principles of hyperspectral imaging technology'. In: Hyperspectral imaging for food quality analysis and control. Elsevier Inc., pp 3–43. https://doi.org/10.1016/B978-0-12-374753-2.10001-2

Fernandes GD et al (2018) Sensory evaluation of high-quality virgin olive oil: panel analysis versus consumer perception. Curr Opin Food Sci 21:66–71. https://doi.org/10.1016/j.cofs.2018.06.001

Furferi R, Governi L, Volpe Y (2010) ANN-based method for olive Ripening Index automatic prediction. J Food Eng 101(3):318–328. https://doi.org/10.1016/j.jfoodeng.2010.07.016

Guillén, R., Fernández-Bolaños, J. and Heredia, A. (1993) 'Evolución de componentes de aceituna (variedad Hojiblanca) durante la maduración', *Grasas y aceites*, 44, pp. 201–203. Available at: http://dialnet.unirioja.es/servlet/articulo?codigo=3938380. Accessed 10 Sept 2020.

Guzmán E et al (2013) Infrared machine vision system for the automatic detection of olive fruit quality. Talanta 116:894–898. https://doi.org/10.1016/j.talanta.2013.07.081

Hussain A, Pu H, Sun DW (2017) (2018) 'Innovative nondestructive imaging techniques for ripening and maturity of fruits – a review of recent applications.' Trends Food Sci Technol 72:144–152. https://doi.org/10.1016/j.tifs.2017.12.010

International Olive Council (2011) 'Guide for the determination of the characteristics of oil-olives', p. 39. Available at: http://www.internationaloliveoil.org/documents/viewfile/5832-co-oh-doc1english.

John GH, Langley P (2013) 'Estimating Continuous Distributions in Bayesian Classifiers'.

Kafkaletou M, Fasseas C, Tsantili E (2019) Increased firmness and modified cell wall composition by ethylene were reversed by the ethylene inhibitor 1-methylcyclopropene (1-MCP) in the non-climacteric olives harvested at dark green stage – Possible implementation of ethylene for olive quality. J Plant Physiol 238:63–71. https://doi.org/10.1016/J.JPLPH.2019.05.006

Kalua CM et al (2007) Olive oil volatile compounds, flavour development and quality: A critical review. Food Chem 100(1):273–286. https://doi.org/10.1016/j.foodchem.2005.09.059

Leiva-Valenzuela GA, Lu R, Aguilera JM (2013) Prediction of firmness and soluble solids content of blueberries using hyperspectral reflectance imaging. J Food Eng 115(1):91–98. https://doi.org/10.1016/j.jfoodeng.2012.10.001

Li B et al (2018) Application of hyperspectral imaging for nondestructive measurement of plum quality attributes. Postharvest Biol Technol 141:8–15. https://doi.org/10.1016/J.POSTHARVBIO.2018.03.008

Liu Q et al (2018) Identification of Bruise and Fungi Contamination in Strawberries Using Hyperspectral Imaging Technology and Multivariate Analysis. Food Anal Methods 11(5):1518–1527. https://doi.org/10.1007/s12161-017-1136-3

Mafra I et al (2001) Effect of ripening on texture, microstructure and cell wall polysaccharide composition of olive fruit (Olea

europaea). Physiol Plant 111(4):439–447. https://doi.org/10.1034/j.1399-3054.2001.1110403.x
Munera S et al (2019) Use of hyperspectral transmittance imaging to evaluate the internal quality of nectarines. Biosys Eng 182:54–64. https://doi.org/10.1016/j.biosystemseng.2019.04.001
Navarro Soto J et al (2018) Fast and reliable determination of virgin olive oil quality by fruit inspection using computer vision. Sensors 18(11):3826. https://doi.org/10.3390/S18113826
Ponce JM et al (2019) Automatic counting and individual size and mass estimation of olive-fruits through computer vision techniques. IEEE Access 7:59451–59465. https://doi.org/10.1109/ACCESS.2019.2915169
Ram T et al (2010) Olive oil content prediction models based on image processing. Biosys Eng 105(2):221–232. https://doi.org/10.1016/j.biosystemseng.2009.10.011
Riquelme MT et al (2008) Olive classification according to external damage using image analysis. J Food Eng 87(3):371–379. https://doi.org/10.1016/j.jfoodeng.2007.12.018
Sun J et al (2016) Multispectral scattering imaging and NIR interactance for apple firmness predictions. Postharvest Biol Technol 119:58–68. https://doi.org/10.1016/j.postharvbio.2016.04.019
Vicente AR et al (2007) The linkage between cell wall metabolism and fruit softening: looking to the future. J Sci Food Agric 87(8):1435–1448. https://doi.org/10.1002/jsfa.2837
Wold S, Esbensen K, Geladi P (1987) Principal component analysis. Chemom Intell Lab Syst 2(1–3):37–52. https://doi.org/10.1016/0169-7439(87)80084-9
Xu D et al (2019) Quantitative Evaluation of Impact Damage to Apple by Hyperspectral Imaging and Mechanical Parameters. Food Anal Methods 12(2):371–380. https://doi.org/10.1007/s12161-018-1369-9
Yu X, Lu H, Wu D (2018) Development of deep learning method for predicting firmness and soluble solid content of postharvest Korla fragrant pear using Vis/NIR hyperspectral reflectance imaging. Postharvest Biol Technol 141:39–49. https://doi.org/10.1016/J.POSTHARVBIO.2018.02.013
Zhang B et al (2014) Principles, developments and applications of computer vision for external quality inspection of fruits and vegetables: a review. Food Res Int 62:326–343. https://doi.org/10.1016/j.foodres.2014.03.012
Zhang C et al (2016) Hyperspectral imaging analysis for ripeness evaluation of strawberry with support vector machine. J Food Eng 179:11–18. https://doi.org/10.1016/J.JFOODENG.2016.01.002
Zhu H et al (2017) Hyperspectral Imaging for Predicting the Internal Quality of Kiwifruits Based on Variable Selection Algorithms and Chemometric Models. Sci Rep 7(1):7845. https://doi.org/10.1038/s41598-017-08509-6
Zhu Q et al (2013) Wavelength Selection of Hyperspectral Scattering Image Using New Semi-supervised Affinity Propagation for Prediction of Firmness and Soluble Solid Content in Apples. Food Anal Methods 6(1):334–342. https://doi.org/10.1007/s12161-012-9442-2